

Regular Article

Characterization of the microstructure of the compositionally complex alloy $\text{Al}_1\text{Mo}_{0.5}\text{Nb}_1\text{Ta}_{0.5}\text{Ti}_1\text{Zr}_1$



J.K. Jensen^a, B.A. Welk^a, R.E.A. Williams^b, J.M. Sosa^a, D.E. Huber^{a,b}, O.N. Senkov^c,
G.B. Viswanathan^a, H.L. Fraser^{a,*}

^a Center for the Accelerated Maturation of Materials, Department of Materials Science and Engineering, The Ohio State University, 1305 Kinnear Rd., Columbus, OH 43212, USA

^b Center for Electron Microscopy and Analysis, Department of Materials Science and Engineering, The Ohio State University, 1305 Kinnear Rd., Columbus, OH 43212, USA

^c Air Force Research Laboratory, Materials and Manufacturing Directorate, Wright-Patterson AFB, OH 45433, USA

ARTICLE INFO

Article history:

Received 10 March 2016

Received in revised form 13 April 2016

Accepted 13 April 2016

Available online 1 May 2016

Keywords:

High entropy alloys

High resolution electron microscopy

Electron tomography

Phase transformations

Ordered compounds

ABSTRACT

Electron microscopy, X-ray energy dispersive spectroscopy, and tomographic reconstructions were used to characterize a high entropy alloy predominantly composed of refractory elements. The intragranular microstructure was found to consist of a periodic two phase mixture, where a disordered *bcc* phase is aligned orthogonally in an ordered B2 phase. The phases were found to exhibit continuous lattice registry and an orientation relationship given by $\langle 100 \rangle_{bcc} // \langle 100 \rangle_{B2}$, $\{001\}_{bcc} // \{001\}_{B2}$. X-ray energy dispersive spectroscopy was used to determine the compositions of the phases, and spectral images were used in the tomographic reconstruction of the alloy to reveal the morphology and the elemental partitioning between phases.

© 2016 Elsevier Ltd. All rights reserved.

In the recent past, multi-principal component or high entropy alloys (HEAs) have garnered significant interest in the field of materials science due to their potentially attractive balance of properties including high compressive strength and corrosion resistance [1–3]. HEAs have been defined as alloy systems composed of five or more principal elements in more or less equiatomic concentrations [4]. The preferential formation of solid solution phases has been observed despite the compositional complexity and was initially attributed to the high configurational entropy of mixing of the constituent elements in the alloy [4]. Other factors including enthalpy of mixing and constituent element atomic size difference, however, influence the stability of solid solutions and many HEA systems have been reported to contain ordered intermetallic phases and complex nanoscale microstructures consistent with phase separation and/or spinodal decomposition [1,5,6]. Because of the uncertainty in the role of entropy on the stability of these alloys, they are referred to here as compositionally complex alloys (CCA).

The development of a novel class of CCAs using predominately refractory elements has been recently explored for potential use in high temperature aerospace structural components [7–9]. One such alloy, $\text{Al}_1\text{Mo}_{0.5}\text{Nb}_1\text{Ta}_{0.5}\text{Ti}_1\text{Zr}_1$ (composition in molar ratio), was reported as having high strength at elevated temperature ($\sigma_{0.2} = 1600$ MPa at $T = 800$ °C, $\sigma_{0.2} = 745$ MPa at $T = 1000$ °C) and a relatively low density

superior to commercially available Ni-base superalloys [8]. Characterization of the alloy was limited to X-ray diffraction (XRD) and scanning electron microscopy (SEM). The alloy was reported to contain two *bcc* phases with similar lattice parameters in a nanoscale interpenetrating microstructure that was difficult to resolve using only SEM micrographs. Since the morphology of these phases and the interconnected nature of the microstructural features are expected to play a substantial role in the deformation behavior and mechanical properties of the alloy, $\text{Al}_1\text{Mo}_{0.5}\text{Nb}_1\text{Ta}_{0.5}\text{Ti}_1\text{Zr}_1$ has been characterized in more detail using transmission electron microscopy and tomographic reconstructions using X-ray energy dispersive spectroscopy (XEDS).

The samples of $\text{Al}_1\text{Mo}_{0.5}\text{Nb}_1\text{Ta}_{0.5}\text{Ti}_1\text{Zr}_1$ used in this study were prepared by vacuum arc melting high purity metals (99.9–99.99%) in an inert argon atmosphere. Details of the alloy preparation are described elsewhere [10]. Following solidification and hot isostatic pressing, the sample was heat-treated at a temperature of 1400 °C for 24 h followed by furnace cooling at a rate of 10 °C/min to room temperature in flowing argon. The microstructure of the heat-treated sample was characterized using backscattered electron (BSE) imaging in an FEI Sirion scanning electron microscope (SEM). Electron backscatter diffraction (EBSD) was performed on CCA samples using an FEI XL-30 FEG SEM equipped with an EDAX Hikari high-speed EBSD camera. SEM and EBSD image processing and analysis was performed using the Materials Image Processing and Automated Reconstruction (MIPAR) software package [11]. TEM lamellae samples were prepared at site specific locations from the surface of the bulk sample, from $\langle 001 \rangle$ oriented grains,

* Corresponding author at: CAMM, The Ohio State University, 1305 Kinnear Rd., Suite 100, Columbus, OH 43212-1177, USA.

E-mail address: fraser.3@osu.edu (H.L. Fraser).

using an FEI Helios NanoLab 600 Dual-Beam focused ion beam (DB-FIB) instrument. The FIB lift-out and thinning procedures are described elsewhere [12].

The thinned FIB lamellae were characterized using conventional bright-field (BF) and dark-field (DF) TEM imaging in an FEI/Phillips CM200. Scanning transmission electron microscopy (STEM) high-angle annular dark-field (HAADF) micrographs were taken with an FEI Probe-Corrected Titan 80-300 STEM operating at 300 kV and a camera length of 115 mm. The convergence semiangle of the electron beam was 11.4 mrad and the inner and outer collection angles of the HAADF detector were 34.8 and 230.0 mrad, respectively. XEDS spectra were collected using an FEI Image-Corrected Titan 60-300 STEM equipped with a Super-X™ XEDS detector system. The TEM was operating with an accelerating voltage of 300 kV and an electron beam convergence semiangle of 25 mrad. Cliff-Lorimer quantification and analysis of Super-X™ XEDS data was performed using standardless native k-factors in the Bruker Esprit software.

The low magnification, BSE micrograph in Fig. 1(a) captures at least two distinct phases, one consisting of equiaxed grains, and the other phase, exhibiting dark contrast, present at some of the grain boundaries of the $\text{Al}_1\text{Mo}_{0.5}\text{Nb}_1\text{Ta}_{0.5}\text{Ti}_1\text{Zr}_1$ sample. EBSD inverse pole figure (IPF) maps overlaid with image quality (IQ) micrographs, shown in Fig. 1(b), show that the equiaxed grains have a *bcc* crystal structure. The identity of the fairly coarse precipitation along the grain boundaries has not yet been confirmed. Low angle subgrain boundaries with misorientation angles of $<1.5^\circ$ are present inside many grains (Fig. 1(a) and (b)). A BSE micrograph (Fig. 1(c)) recorded at higher magnification reveals fine precipitation of two phases in the equiaxed grains. These precipitates form a basket weave nanoscale structure inside the grains and become coarser at subgrain boundaries. The intragranular microstructure is identified by TEM to consist of a refined distribution of two interpenetrating phases, which appear to have a lamellar morphology (Fig. 1(d)).

Previously, the microstructure was characterized as consisting of two interpenetrating *bcc* phases [8]. As can be seen in Fig. 1(d), the selected area diffraction pattern (SADP) exhibits intensity maxima that appear to be superlattice reflections. Indeed, the DF-TEM micrograph of the refined, interpenetrating microstructure shown in the figure was recorded using the reflection circled in the diffraction pattern (inset), with the electron beam being nearly parallel to a $\langle 001 \rangle$ zone axis. As can be seen, the microstructure appears to consist of a refined distribution of one phase, exhibiting dark contrast and consisting of cuboidal and stacked platelet precipitates ~ 40 nm in edge length, aligned along $\langle 100 \rangle$ directions, within a lighter contrast phase. Since the image is formed with an intensity maximum consistent with a superlattice reflection, it appears that the lighter phase is ordered. Given the locations of the superlattice reflections in this and other zone axes SADPs (not shown here), it is reasonable to conclude tentatively that the phase has the B2 crystal structure. In the SADP (Fig. 1(d)), the fundamental intensity maxima from both phases are coincident, and hence, within the error of measurement using SADPs, it appears that both phases have lattice parameters of ≈ 0.329 nm, indicating a reasonable degree of coherency between the two phases.

Fig. 2 (a and b) shows STEM-HAADF micrographs acquired with the electron beam parallel to the $[001]$ zone axis of the *bcc*/B2 phases. The microstructure consists of two phases: one a cuboidal and plate-like precipitate phase, exhibiting grey contrast, aligned orthogonally in a phase which exhibits darker contrast. In STEM-HAADF imaging conditions, contrast arises from the collection of incoherently scattered high-angle electrons and, therefore, from variations in local atomic number between phases [13]. It follows that the grey phase has a higher average atomic number than the darker phase, as is confirmed by compositional analyses below. Fig. 2(b) shows a higher magnification STEM-HAADF image resolving atomic columns, in which the modulation of intensity from the corner site to the body centered site in the darker phase (i.e., the ordered phase) can be seen clearly. This is indicative of a

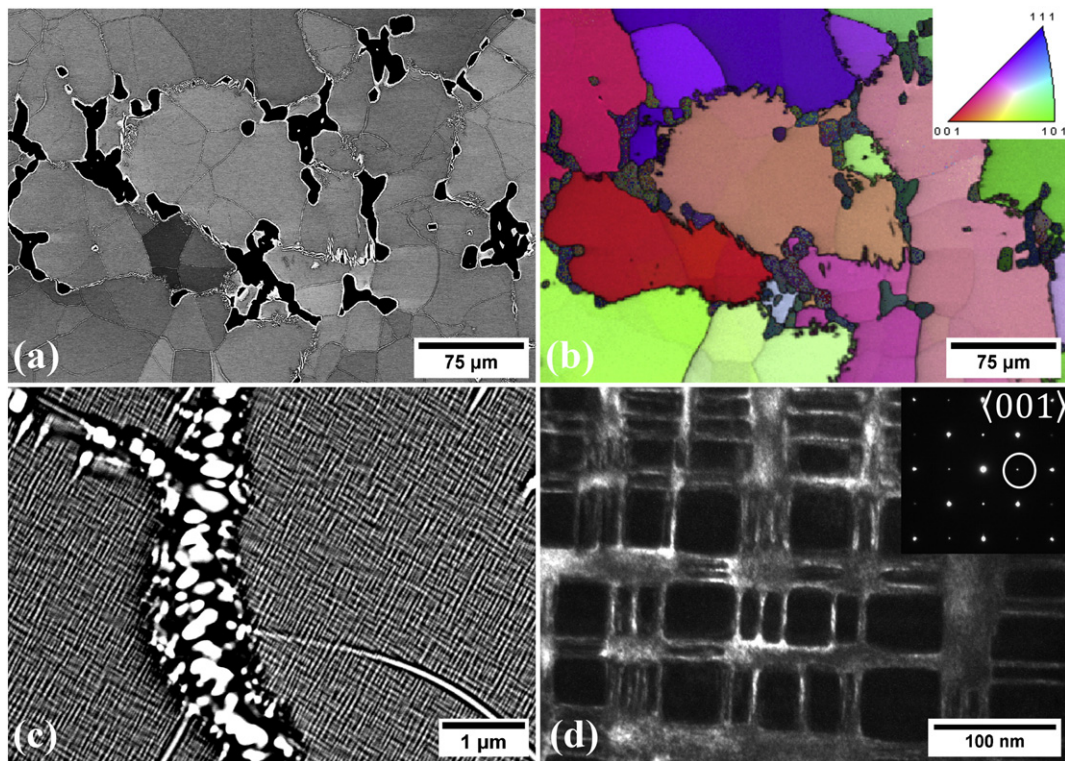


Fig. 1. (a) SEM BSE micrograph of the microstructure of $\text{Al}_1\text{Mo}_{0.5}\text{Nb}_1\text{Ta}_{0.5}\text{Ti}_1\text{Zr}_1$ showing coarse grains, with intragranular features and dark intermetallic phases at the grain boundaries; (b) EBSD inverse pole figures with overlaid image quality map identifying the intragranular features as low angle subgrain boundaries; (c) SEM BSE micrograph showing intragranular microstructure near a low angle subgrain boundary; (d) TEM darkfield micrograph formed using the intensity maxima circled in the selected area diffraction pattern (inset).

Download English Version:

<https://daneshyari.com/en/article/1498007>

Download Persian Version:

<https://daneshyari.com/article/1498007>

[Daneshyari.com](https://daneshyari.com)